Research Article

Role of Tin Metal in Red Visible Light in Diesel Oil Desulfurization Process with Looping Process System

Dino Dewantara and Ismail
Master Program of Chemical Engineering, Faculty of Engineering, Universitas Sriwijaya, Ogan Ilir, Indonesia

Muhammad Djoni Bustan* and Sri Haryati
Department of Chemical Engineering, Faculty of Engineering, Universitas Sriwijaya, Ogan Ilir, Indonesia

* Corresponding author. E-mail: muhammaddjonibustan@ft.unsri.ac.id DOI: 10.14416/j.asep.2025.01.006
Received: 4 December 2024; Revised: 6 January 2025; Accepted: 21 January 2025; Published online: 31 January 2025

Abstract
The conventional desulfurization process requires a considerable quantity of materials. It presents a significant challenge to control, both of which contribute to a higher cost of production for low-sulfur diesel fuel. The utilization of red visible light, a clean and environmentally health-friendly form of energy and can be employed under low operating conditions, represents an adequate substitute for the promising diesel oil desulfurization process. The potential of metallic catalysts to enhance the properties of red visible light in the desulfurization process was investigated. The red visible light desulfurization process demonstrated that diesel oil can be reduced in sulfur content under ambient operating conditions. The highest yield in this study was achieved at a catalyst height variation of 6 cm and an irradiation time of 25 h with a sulfur content of 737 ppm. Tin metal significantly enhances red visible light's photon energy, frequency, wavelength, and minimum kinetic energy.

Keywords: Desulfurization process, Diesel, Red visible light, Sulfur reduction, Tin metal

1 Introduction

Community activities such as vehicle use, forest burning for land clearing, and industrial processes are significant sources of pollutants to society. If left unchecked over a long period of time, these pollutants will have detrimental effects. Most of these pollutants come from the use of fossil fuels, such as petroleum. Fossil fuels remain the primary natural resource used to meet the enormous energy needs of contemporary society. Projections show that energy consumption will continue to rise until 2040, mainly due to the expansion of the global population which is expected to reach 1.7 billion [1].

These pollutants must be reduced gradually. One such reduction method is the reduction of sulfur pollutants in vehicles [2]. Many types of pollutants are emitted by cars, including CO, CO_2, and SOx gases. During the combustion process in the engine, these gases are emitted and contribute greatly to environmental pollution [3]. In addition, toxic sulfur oxide (SOx) gas emissions can lead to the formation of smog and precipitation, as well as the release of odorous compounds that can cause headaches and eye irritation [4]. However, diesel oil, which is the main source of sulfur oxide (SOx) emissions, continues to increase on a global scale, from 99 million barrels per day (b/d) in 2022 to 101 million barrels per day (b/d) in 2023. This trend is projected to continue [5].

The desulfurization process is a considerable challenge to reduce sulfur content in the petrochemical industry, especially in liquid fuel products such as diesel. Petroleum products, in particular, contain various sulfur-containing compounds, including thiols, thiophenes, benzothiophenes (BT), dibenzothiophenes (DBT), and 4,6-dimethylbenzothiophenes (4,6-DMBT). These compounds are present in liquid fuels and contribute to the overall sulfur content. Therefore, it is imperative to develop efficient desulfurization technologies capable of removing sulfur compounds from fuels in accordance with today's stringent environmental regulations [6]–[9]. Technologies such

as hydrodesulfurization sulfur (HDS), biodesulfurization, extractive desulfurization sulfur (EDS), adsorptive desulfurization sulfur (ADS), and oxidative desulfurization sulfur (ODS) have been widely applied for desulfurization of fuel oil but have disadvantages such as the use of many raw materials such as catalysts and additives and the operating conditions are still very high, making it ineffective in application to industrial processes [10]–[18]. Therefore, there is a need to update the desulfurization process from conventional methods to be industrialized at a low cost but still efficient and effective with mild operating conditions.

Light energy is an interesting phenomenon that can be utilized for a variety of applications. Its unique qualities make it an ideal candidate for renewable energy sources as it operates effectively under low-level conditions and requires minimal maintenance. Therefore, efficient and effective utilization of light energy has emerged as a very important research topic, with the potential to revolutionize industrial processes and energy production while promoting environmental sustainability [19]–[21].

The desulfurization process using light has been applied with UV light, as done by Gondal *et al*. who conducted research on desulfurization of dimethyl-dibenzothiophene (DMDBT) by utilizing ArF laser light energy using UV light with additional oxygen assistance. In the process after being irradiated, DBT and O_2 will form endoperoxia which is more thermally labile and easily decomposed to release sulfur where operating conditions are at room temperature [22].

Shinozaki *et al*. conducted the decomposition of BT and DBT derivatives induced with ultraviolet light. This study used UV light with a wavelength of 254 nm at a power of 8 W at 25 °C for 24 h. The formation of sulfur allotropes characterized the sulfur reduction of BT and DBT. The results showed that DBT can be decomposed by producing sulfur precipitates [23].

However, the use of UV light imposes a burden on controlling the process. Using UV generators with high-pressure xenon light or mercury light is relatively expensive. In addition, direct exposure to UV light can cause blindness and skin cancer, making it difficult to apply to industry. Therefore, a more cost-effective and safe alternative is needed that can provide comparable results while ensuring human health safety.

One of the visible light rays that has attracted attention is red light, which has been used in various processes with significant effects. In photopolymerization processes, visible light, such as orange light and red light, provides increased bond penetration, high initiation efficiency, and low process costs [22]. Visible light causes chemical reactions to take place under mild conditions compared to UV light [23]. Red light on photocatalysts prevents the occurrence of unwanted by-products [24]–[26].

The potential of red light as an energy source for organic reactions has recently attracted the attention of organic chemists, mainly due to its safety profile. In addition to the widely used singlet oxygen uptake [27], [28], there has been a recent increase in research investigating red light-mediated organic transformations involving photo-redox mechanisms or intramolecular charge transfer [29]–[31]. Ogura *et al*. examined the Barton-McCombie reaction mediated by red light [32]. The results showed that in the presence of chlorophyll a as a catalyst and tris(trimethylsilyl)silane or Hantzsch ester as a hydrogen source, xanthine methyl groups were removed by red light irradiation. The reaction mechanism is probably via complex formation between the substrate and the photocatalyst, followed by charge transfer. These operating conditions are considered safer and more efficient than conventional operating conditions [33].

This research will review the desulfurization process by utilizing red visible light with continuous looping flow to reduce sulfur content in diesel oil through a process that is cheaper and safer and can be easily implemented in industries where the use of red light directly in the reaction process has not been specifically studied.

In addition, a light energy amplification process was developed by applying a metal catalyst-assisted process to the light. The incorporation of metal facilitates the photoelectron effect, which allows the collision of photons on the surface of the substance (solid metal) to stimulate electrons, thereby increasing the expansion of the sulfur solution in diesel oil [34], which has never been studied in various types of desulfurization processes.

2 Materials and Methodology

2.1 *Material*

The diesel oil is from PT Kilang Pertamina International, RU III Plaju refinery, Indonesia. The 700 nm red light is from Dongguan HouKe Electronic Co. Ltd, China, and Sn metal is from Palembang, Indonesia.

2.2 *Diesel oil desulfurization process*

The sequence of steps in this process is illustrated in Figure 1. The diesel oil feedstock is stored in a tank. Diesel oil is then flowed into the desulfurization reactor through a centrifugal pump equipped with a flowmeter. Diesel oil will then enter through the inlet of the desulfurization reactor and then flow into the reactor with a volume of 30 mL. Previously, tin catalyst in powder form was placed on the catalyst bed with variations in catalyst height of 2, 4, and 6 cm to see the effect of the amount of tin catalyst on energy enhancement in red light. The catalyst bed is under the reactor tube so there is no direct contact with the reactants. The light will first pass through the catalyst before irradiating the diesel oil in the reactor tube. In the desulfurization reactor, the diesel desulfurization process will occur with the help of a red light that has previously been in contact with the tin catalyst and then enters and illuminates the desulfurization reactor area. The desulfurized diesel flow then exits through the reactor outlet and is circulated by flowing to the mixing valve to flow back into the desulfurization reactor so that it will produce a continuous looping process flow. The red light source is powered by electricity through a DC adapter. The continuous looping flow process will be stopped according to the variation of red light irradiation time with variations of 1, 3, 5, and 10 h for the 20 W power variation and 1, 5, 10, 15, 20, and 25 h at the 50 W power variation and then the product can be taken through mixing valve 2.

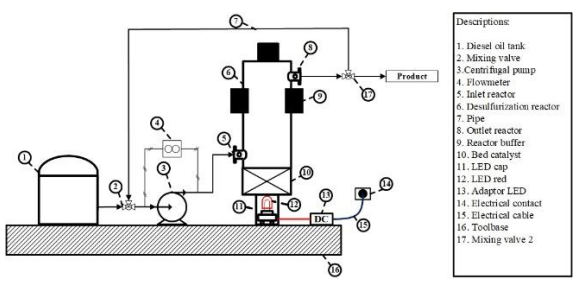

Figure 1: Schematic of diesel oil desulfurization process with tin metal catalyst-assisted red visible light.

2.3 *Sulfur content analysis and characterization of diesel oil*

Sulfur reduction analysis in diesel oil was performed using Panalytical Epsilon 3X equipment with X-ray fluorescence (XRF) methodology at 30 kV. In addition, Fourier transform infrared (FTIR) spectroscopy, using a DW-FTIR-530 spectrometer, was used to characterize the diesel oil samples before and after irradiation.

3 Results and Discussion

3.1 *Desulfurization of diesel oil at various times and catalyst heights at 20 W red light power*

The diesel oil desulfurization process uses raw materials from the PT Pertamina RU III Plaju refinery, Indonesia, with a sulfur content of 1300 ppm. The reactor volume used in this study was 30 mL with a continuous looping process. The results of desulfurization at 20 W red light power are illustrated in Figure 2. The variables used in this process include irradiation times of 1, 3, 5, and 10 h, as well as tin (Sn) catalyst heights of 2, 4, and 6 cm, in addition to variations without using catalysts.

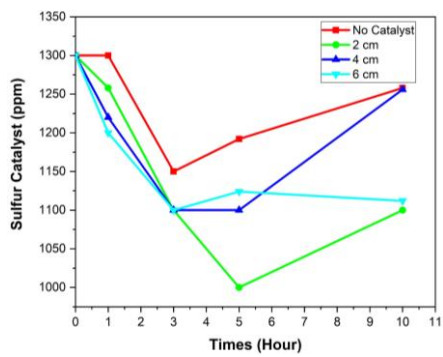

Figure 2: Desulfurization results of diesel oil with a variation of time and catalyst height at 20 W red light power.

Without a tin catalyst, the desulfurization process showed sulfur content ranging from 1000 to 1300 ppm. It was observed that, over an hour, no sulfur reduction occurred. The addition of a catalyst to enhance the absorption of red visible light has the effect of accelerating the desulfurization process in diesel oil. As illustrated in Figure 2, the incorporation of the Sn catalyst facilitates the desulfurization process of diesel oil. The lowest sulfur content was achieved using a 6 cm Sn catalyst for 3 h at 1100 ppm and 10 h at 1112 ppm. The use of 2 cm and 4 cm catalysts showed a decrease in sulfur content. However, the results showed variability related to irradiation time. In the case of the 2 cm catalyst variation, the lowest sulfur content was observed at 5 h, with a concentration of 1000 ppm. In contrast, the 4 cm catalyst variation showed the lowest sulfur

content at time points 3 and 5 h, with a concentration of 1100 ppm.

Figure 3 illustrates the results of sulfur reduction in the diesel oil desulfurization process with a power variation of 20 W. These results are in agreement with those presented in Figure 2. Specifically, the highest sulfur reduction was observed with the 6 cm catalyst variation, with a reduction of 100–200 ppm. In contrast, the lowest sulfur reduction was observed without a tin catalyst, with a decrease of 0–150 ppm.

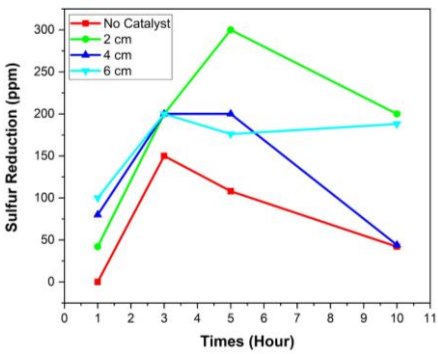

Figure 3: Graph of sulfur reduction in 20 W red visible light power desulfurization.

3.2 *Desulfurization of diesel oil at various times and catalyst heights at 50 W red light power*

The samples showed better results when irradiated by red light with a power of 50 W. In this experimental setup, the radiation time was varied more extensively, including 1, 3, 5, 10, 15, 20, and 25 h, with the height of the catalyst undergoing corresponding changes, namely 2, 4, and 6 cm. As illustrated in Figures 4 and 5, the sulfur content of the 50 W power variation was observed to be lower, ranging from 737 to 1298 ppm. The lowest sulfur content, 737 ppm, was observed in the 6 cm Sn catalyst height variation with an irradiation time of 25 h, corresponding to a sulfur reduction of 563 ppm. The 6 cm catalyst height variation showed the lowest average sulfur content and the highest sulfur reduction, ranging from 737 to 1105 ppm with sulfur reduction of 124 to 563 ppm.

In the absence of Sn catalyst, sulfur reduction remained relatively low, with average sulfur content exceeding 1200 ppm and sulfur reduction of only 2–196 ppm. These findings suggest that the addition of Sn increases the red visible light energy, as evidenced by the increased desulfurization yield observed with varying catalyst heights (2, 4, and 6 cm). Therefore, further investigation into the impact of Sn catalysts on visible light enhancement in the desulfurization process is required.

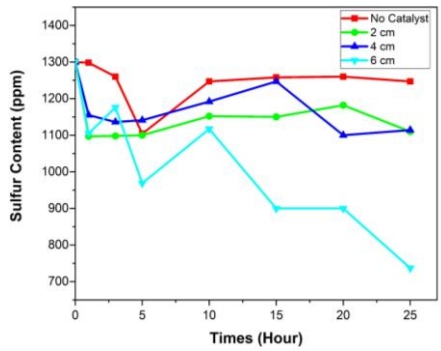

Figure 4: Desulfurization results of diesel oil with a variation of time and catalyst height at 50 W red light power.

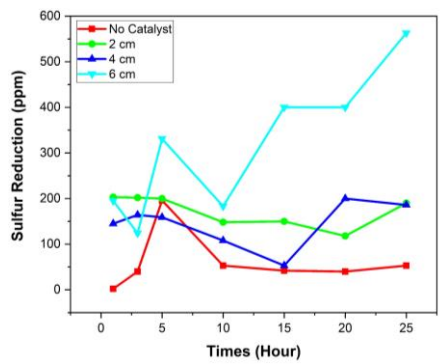

Figure 5: Sulfur reduction in 50 W red visible light power desulfurization.

3.3 *The effect of tin metal in increasing the photon energy of red visible light*

Based on the principles of modern quantum optics theory, rays are considered to be electromagnetic waves and collections of particles, referred to as photons, that travel at the speed of rays in a vacuum. Each photon is a quantum of electromagnetic energy and is considered a discrete particle with zero mass, no charge, and infinite lifespan. Upon interacting with an object, the photon transfers its power to the object, attracting electrons in the ground state of the molecule. These electrons then transition to a higher energy level. Furthermore, when the excited electrons return to a lower energy level, the molecule emits light as a photon with a specific wavelength and energy quantum [35].

Photons can be described as electrons in a state of motion within a light, which allows them to emit

radiation. Photons in red visible light in this study can be enhanced by utilizing photoelectron events with the use of tin metal catalysts.

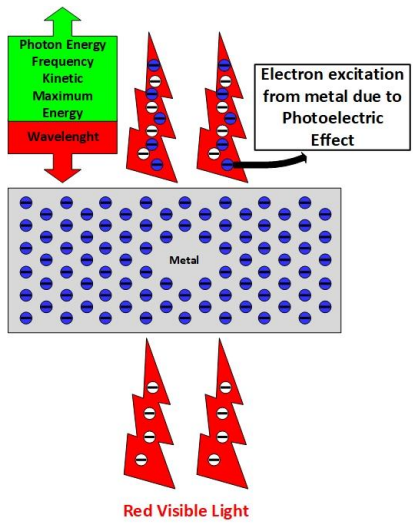

Figure 6: Tin metal electron excitation mechanism due to photoelectron event by the propagation of red visible light on the metal.

The presence of electrons in metals can affect the energy of photons, as electrons can be removed or extracted when exposed to energy from heat due to the collision of electromagnetic radiation of red visible light. During this process, red light is transmitted into the metal, interacting with the electrons, causing them to generate heat. This heat then extracts electrons from the metal which ultimately increases the electron density of the light. The increase in electrons in red light due to the addition of excited electrons from the tin metal causes an increase in the photon energy in red light, so it will facilitate the cracking process of the bonding of sulfur compounds such as DBT with hydrocarbons in diesel oil. The mechanism of the photoelectron process in red visible light with metals is presented in Figure 6.

To review the effect of tin metal in increasing the energy of red visible light photons, the following formula will be used:

$$E_p = h. \quad (1)$$

$$E_p = \frac{h\,c}{\lambda} \quad (2)$$

$$E_{kmax} = E_p - E_0 \quad (3)$$

E_p is the photon energy (eV), h is the plack constant (6.63×10^{-34} J s^{-1}), f is the frequency (Hz), c is the light velocity (3×10^8 m s^{-1}), λ is the wavelength (nm), E_{kmax} is the maximum kinetic energy kJ mol^{-1} and E_0 is the metal threshold energy (kJ mol^{-1}) [36], [37]. Equations (1) to (3) are used to determine the photon energy, frequency, wavelength, and maximum kinetic energy in red light when irradiating diesel oil. The results of 50 W power variation showed superior performance compared to the results obtained at 20 W power. Therefore, the role of tin metal in red visible light will be studied by utilizing the results of 50 W power diesel oil desulfurization.

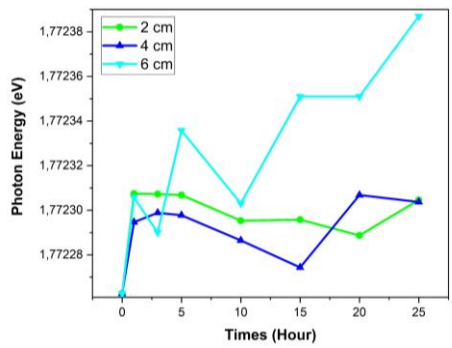

Figure 7: Changes in energy photons of red visible light at varying catalyst heights.

The visible red light used in this study has a wavelength of 700 nm. This serves as the basis for calculating photon energy and subsequent parameters. The initial photon energy of visible red light is 1.772263 eV, which will increase with the influence of red light power, irradiation time, and the use of tin catalyst. The use of tin metal has been observed to increase the photon energy of visible red light, which is in line with the desulfurization results. The 6 cm catalyst height variation shows the highest increase in photon energy, which is 1.772387 eV with an increase of 0.007% from the initial photon energy, with the highest result occurring in the 25 h time variation, as shown in Figure 7. The increase in photon energy with the increasing number of catalysts identifies the occurrence of photoelectron events on tin metal due to the propagation of red light before irradiating diesel oil. More catalysts provide more electron supply for the red visible light resulting in higher electron density. Increasing the duration of red light irradiation results in prolonging the contact between the red light and diesel oil. Consequently, the cracking process of sulfur compounds with hydrocarbons in DBT is accelerated, as evidenced by the results obtained. The

longest irradiation time of 25 h gave the highest results.

3.4 *The effect of tin metal on the frequency of light appears red*

The frequency of the light is directly correlated to the photon energy, with higher photon energy resulting in higher light frequency. The addition of metal in this study increases the photon energy in the light, thereby increasing the frequency and reducing the initial light wavelength. This will increase the interaction rate of the light and diesel oil, thus accelerating the cracking process of hydrocarbon bonds with sulfur compounds in diesel oil by red visible light.

In addition to the increase in photon energy associated with the use of tin metal catalysts, there is an observable increase in the frequency of red visible light. As illustrated in Figure 8, the initial frequency of red visible light before the addition of the tin metal catalyst was 4.28502×10^{14} Hz and then increased with the addition of the catalyst. The catalyst height variation of 2 cm shows an increase in frequency to 4.28508×10^{14} Hz and further to 4.28513×10^{14} Hz. The catalyst height of 4 cm showed a frequency range of 4.28505×10^{14} Hz to 4.28513×10^{14} Hz. The highest results were observed in the 6 cm variation, with a maximum frequency of 4.28532×10^{14} Hz.

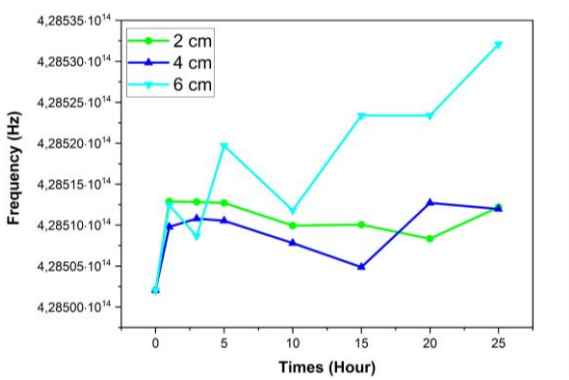

Figure 8: Changes in red visible light frequency at varying catalyst heights.

The frequency of visible red light increases due to the introduction of electrons in the light as it passes through the metal catalyst, which triggers what is known as a photoelectron event [34]. This phenomenon is characterized by the release of electrons within the metal itself. The resulting electron spike causes an increase in the electron density within the light, resulting in high electron frictional motion and an overall increase in the frequency of the visible red light.

Frequency is an important cornerstone in the ease of cracking hydrocarbon bonds with sulfur compounds in diesel oil. The higher frequency will accelerate the collision process of the light with the cracking so that the reaction process can take place faster.

3.5 *Effect of tin metal on the wavelength of red visible light*

A ray is a form of electromagnetic radiation that exhibits both particle and wave properties. Waves of electromagnetic radiation have a unidirectional vector, which is determined by three main characteristics: wavelength (λ, the distance between successive peaks), frequency (oscillations per second), and amplitude (the difference between valleys and peaks). Energy particles in electromagnetic radiation include photons, which travel at a speed of 3×10^9 m per second. As a result, the wave mixture will consist of photons traveling with different amplitudes and frequencies that are scattered and absorbed. It can be reflected by various objects, including biological materials [38].

Rays that show a narrow band of rays with a single color are classified as monochromatic rays. The wavelength range for monochromatic rays is often designated as violet (380–450 nm), blue (450–495 nm), green (495–570 nm), yellow (570–590 nm), orange (590–620 nm), or red (620–750 nm). In the visible light spectrum, violet light has the shortest wavelength, which corresponds to the highest frequency and energy. Conversely, red has the longest wavelength, lowest frequency, and lowest energy of all the colors in the spectrum [39].

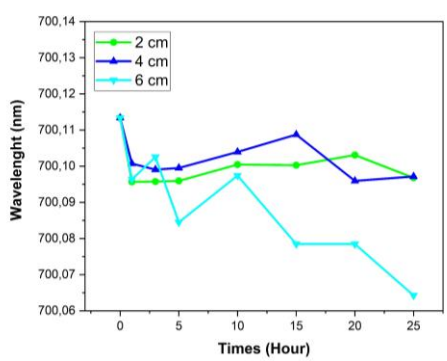

Figure 9: Change in wavelength of red visible light at various catalyst heights.

An increase in frequency leads to a decrease in the wavelength of visible red light, as evidenced by the relationship between the two parameters. This phenomenon can be attributed to the accelerated movement of electrons, which effectively reduces the distance traveled by visible red light. The wavelength of red light passing through diesel oil is initially 700.1134 nm. Upon propagation of red light into the tin metal catalyst, there is a noticeable decrease in wavelength. This phenomenon is illustrated in Figure 9, which depicts the wavelength variations observed in catalysts of different heights, especially in the 2 cm height range, where the wavelength drops from 700.0957 nm to 700.1031 nm. The 4 cm catalyst height variation shows a wavelength range of 700.0971 to 700.1087 nm. The 6 cm catalyst height variation showed the lowest wavelength achieved at 25 h time variation with a wavelength of 700.0643 nm, showing a decrease in wavelength by 0.0388 nm.

3.6 *Effect of tin metal in increasing the maximum kinetic energy of red visible light*

The threshold energy provides the basis for determining the light photon energy required to facilitate the extraction of electrons from the metal in question. It should be noted that each metal has a unique threshold value, which serves as a benchmark to determine the efficacy of the light in extracting electrons from the metal. To ensure the successful extraction of electrons from metals, the light must have a photon energy that matches or exceeds the above threshold energy. The maximum kinetic energy of a photon represents the difference between the photon energy and the threshold energy. A higher maximum kinetic energy implies that the photon energy of the light exceeds the threshold energy of the metal.

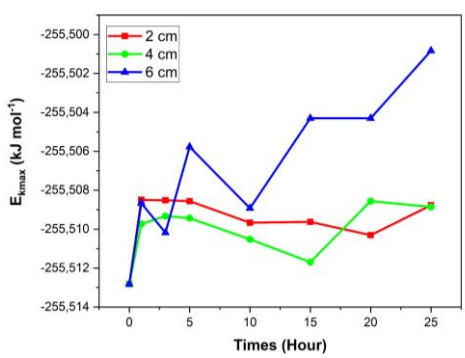

Figure 10: Changes in the maximum kinetic energy of red visible light at varying catalyst heights.

The threshold energy of the Sn metal catalyst is 4.42 electronvolts (eV), equivalent to 426 kJ mol^{-1}. This value is the reference point for calculating the maximum kinetic energy generated when red visible light propagates into the tin metal catalyst. As illustrated in Figure 10, the use of a tin catalyst shows a higher maximum kinetic energy, with the most obvious result seen in the 6 cm catalyst height variation, which reaches –255.501 kJ mol^{-1} with an increase of 0.004% and the lowest maximum kinetic energy of –255.512 kJ mol^{-1} achieved in the 4 cm catalyst height variation. The 2 cm catalyst height variation showed the maximum kinetic energy in the range of –255.510 kJ mol^{-1} to –255.508 kJ mol^{-1}. The 4 cm catalyst height variation produces maximum kinetic energy in the range of –255.512 kJ mol^{-1} to –255.509 kJ mol^{-1}.

3.7 *Characterization analysis of desulfurized diesel oil*

A detailed examination of the composition of diesel oil is essential to ascertain the changes brought about by the desulfurization process. For this purpose, Fourier-transform infrared (FTIR) spectroscopy will be used. The selected samples exhibit varying reaction times: 5, 15, and 25 h at a catalyst height of 6 cm. These samples were selected based on the most significant desulfurization results. Samples before irradiation were also studied to compare the results.

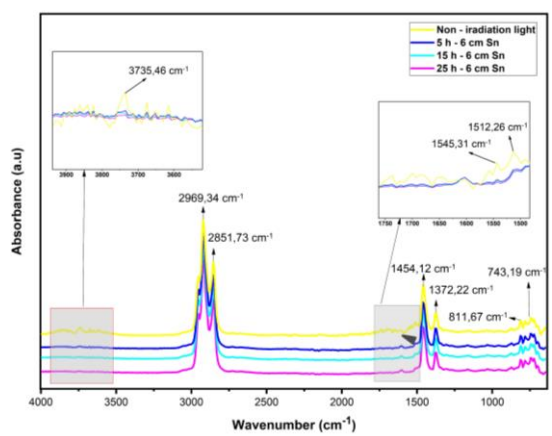

Figure 11: FTIR characterization of diesel oil before and after red visible light irradiation.

Fourier transform infrared (FTIR) analysis was used to ascertain the changes in functional groups before and after exposure to red light, as illustrated in Figure 11. As illustrated in the FTIR result for peak 2851.73 cm^{-1}, symmetrical stretching of the CH, CH_2,

and CH_3 functional groups was observed, while asymmetrical stretching of the same functional groups was seen in the FTIR result for peak 2969.34 cm^{-1} [40], [41]. The peak at 1454.23 cm^{-1} indicates asymmetric deformation of the CH, CH_2, and CH_3 bonds and the peak at 1372.22 cm^{-1} indicates deformation of the C-O bond. In addition, the peaks observed at 811.67 cm^{-1} and 743.19 cm^{-1} indicate out-of-plane C-H bands [42]. These functional groups are the main constituents of diesel and are present in all samples.

In the diesel oil samples that were not irradiated with red light, distinct peaks were observed. In contrast, these peaks were not present in the sample that had been irradiated with red light. The peaks were identified as 1,545.31 cm^{-1} and 1,512.26 cm^{-1}; the former indicates a C-S stretching peak [43], while the latter indicates an O-H stretching peak [44]. The peaks in question indicate the presence of sulfur compounds, a change that was observed when the above sample was irradiated. This indicates that the sulfur compounds undergo a reaction process into endoperoxide compounds, in this case dibenzosulfonate ($DBTO_2$) due to the reaction between DBT and the oxygen content of diesel oil, which will be easier to separate from diesel oil by various separation processes [22], [23].

3.8 *Theoretical study of sulfur compound decomposition mechanism from diesel oil with DFT*

The DFT method can be used to explain the reaction mechanism that occurs in the desulfurization process of diesel oil. The sulfur compound chosen in this process is DBT, which is the most dominant sulfur compound in diesel oil. All DFT calculations in this study used Gaussian 5, and the results were visualized using Gaussview [23].

The first step in this process was to study how DBT compounds can be released from their bonds with hydrocarbons in diesel oil by cracking under red visible light. Diesel fuel production is a multistage process involving fractional distillation of crude oil under temperature conditions between 200 °C and 350 °C. Its chemical composition includes 64% by weight of aliphatic hydrocarbons, with most of the carbon amounts in the C9–C20 range, 35% by weight of aromatic hydrocarbons, which include benzene and polycyclic aromatic hydrocarbons, as well as a small proportion of olefinic hydrocarbons, which is estimated to be between 1–2%.

To represent the DFT calculation process for the cracking reaction of aliphatic hydrocarbon bond breaking and DBT in diesel oil, C9 aliphatic will be used, and benzene is chosen to represent DBT bonding with aromatic hydrocarbon. The methodology used is spin-flip time-dependent (TD) DFT (B3LYP/6-31G*) [23]. The interaction results show that the C9 aliphatic hydrocarbon bond with DBT has an energy value of –1213.7849 a.u. The highest occupied molecular orbital or HOMO (Highest Occupied Molecular Orbital) generated by this bond is –0.20671 a.u. Conversely, the lowest unoccupied molecular orbital or LUMO (Lowest Unoccupied Molecular Orbital) is –0.03870 a.u, where the resulting HOMO-LUMO is –0.16801 a.u.

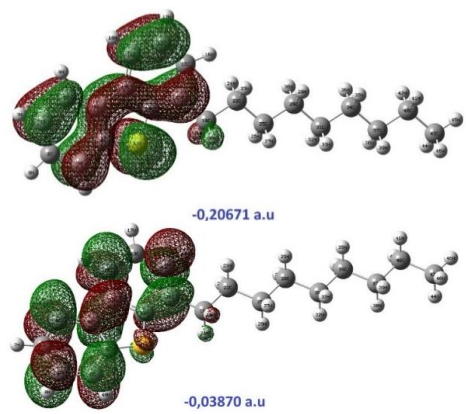

Figure 12: HOMO and LUMO profile of C9-DBT.

The lowest HUMO and LUMO states of this compound bond were observed at the closest carbon bond between C9 and DBT, especially at carbon number 19 (Figure 12). This indicates that the region has an antibonding Molecular Orbital (MO) lobe, which allows the process of breaking the aliphatic bond between C9 and DBT due to electron transfer by red light. This antibonding character has the potential to interact with electrons from outside, in this case, red light, which will trigger bond changes because antibonding properties can weaken the bonds that already exist in this molecule.

In the case of the Benzene-DBT bond, slightly different results were observed in this aromatic bond with DBT. The energy generated in this structure is more than –1091.0461 a.u. This is because this structure has fewer atoms than the aliphatic C9-DBT bond. For the HOMO and LUMO structures of benzene-DBT, the results are –0.21085 a.u. and –0.05289 a.u., with a HOMO-LUMO value of –0.15796 a.u. (Figure 13 and Table 1).

Table 1: Molecular orbital energies of HOMO and LUMO in hydrocarbon bonds with DBT.

Compound	HOMO (a.u)	LUMO (a.u)	HOMO - LUMO (a.u)
C9 - DBT	–0,20671	–0,03870	–0,16801
Benzene - DBT	–0,21085	–0,05289	–0,15796

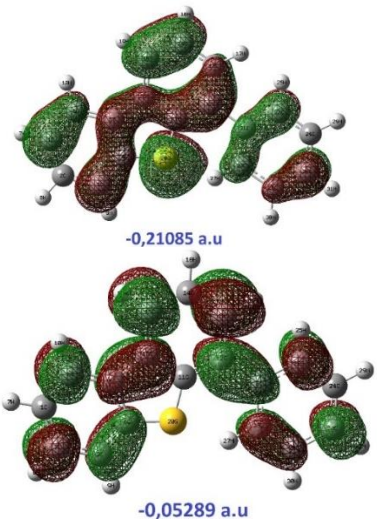

Figure 13: HOMO and LUMO profiles of Benzene - DBT.

The region that will be involved in the reaction is the LUMO region, which tends to accept electrons due to its unfilled orbital state. The LUMO region on the benzene-DBT bond is lower than the LUMO region on the C9-DBT bond, –0.03870 a.u > –0.05289 a.u. As a result, DBT tends to be more easily released via aromatic bonds than aliphatic bonds. As illustrated in Figure 4, the HOMO and LUMO in the benzene and DBT structures show concentrated strength in each structure. As a result, when the carbon atoms at positions 12 and 21 interact with electrons in the external environment, these bonds will quickly detach. In contrast, the HOMO and LUMO structures in the C9-DBT aliphatic bond show greater concentration in the DBT area compared to the C9 aliphatic area, so it will be more difficult to release.

Weak bond energy plays a role in the cleavage of DBT bonds with hydrocarbons in diesel oil. In comparison, the aromatic benzene-DBT bond, which shows a lower breaking energy compared to the aliphatic C9-DBT bond, requires a breaking energy of 114,864.82 kcal/mol, while the aliphatic C9-DBT bond requires a higher breaking energy 221,883.91 kcal/mol (Figure 14).

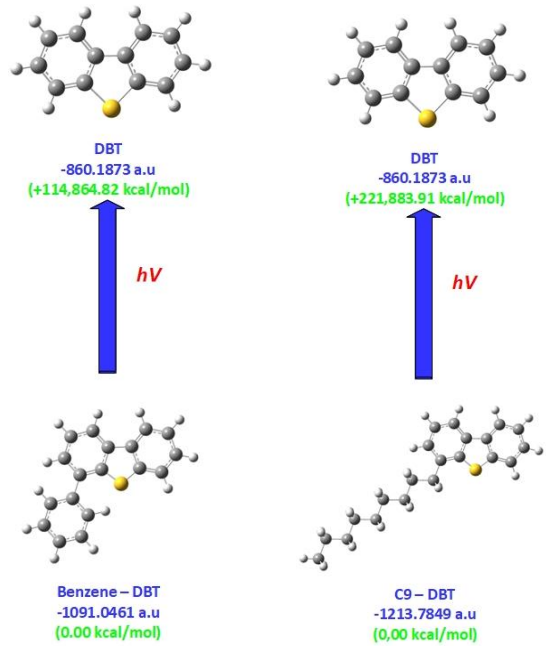

Figure 14: DBT desulfurization energy profile of hydrocarbon - DBT bonds.

The next stage is the conversion of DBT to $DBTO_2$, an endoperoxide compound. After bond breaking, the endoperoxide compound $DBTO_2$ will be easier to separate from the hydrocarbon. The DBT compound will be difficult to separate if it is not in the form of $DBTO_2$ because its boiling point ranges from 332 to 333 °C, which is close to the boiling point of diesel oil composition (between 163 °C to 357 °C). In contrast, the boiling point of $DBTO_2$ is much higher, reaching 422 °C. In addition, the formation of $DBTO_2$ through the reaction of DBT with the oxygen source in diesel oil also inhibits the reverse reaction of DBT to bind back to hydrocarbons.

In addition to the hydrocarbons and sulfur compounds that characterize diesel oil, this fuel contains various other chemical constituents, including oxygen. In this $DBTO_2$ formation mechanism, DBT that has been separated from hydrocarbons will react with oxygen present in diesel oil, facilitated by red light. The application of red light will encourage the formation of reactive DBT compounds, namely triplet excited state (T1), through the excitation process of DBT.

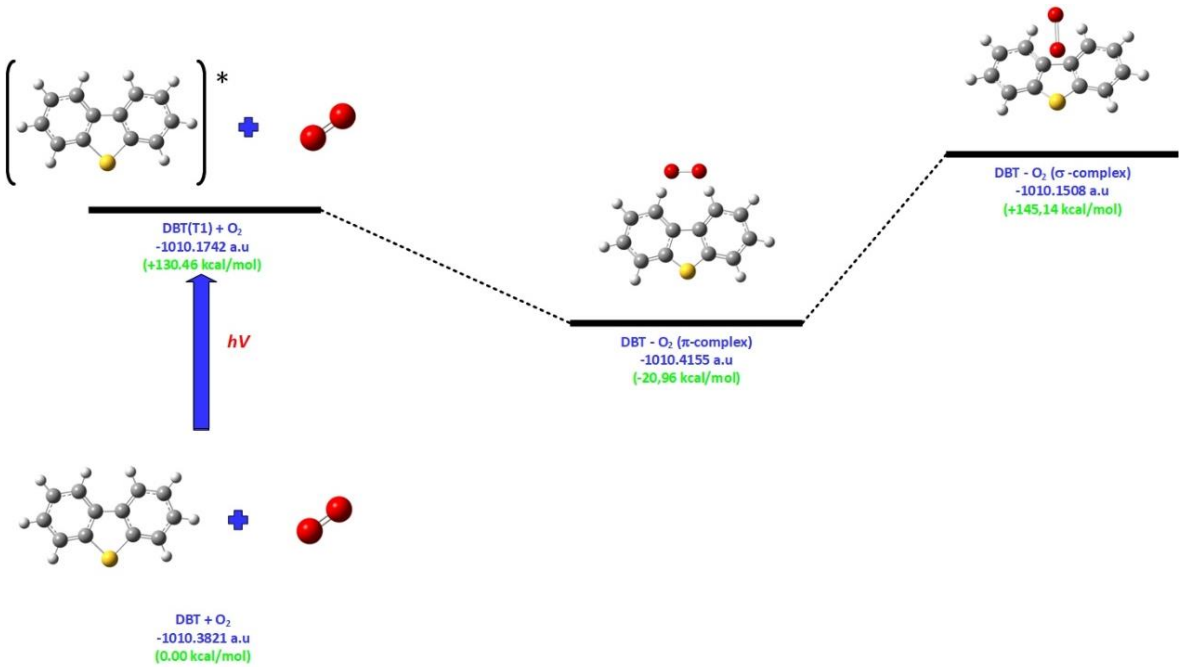

Figure 15: Formation of DBT into $DBTO_2$.

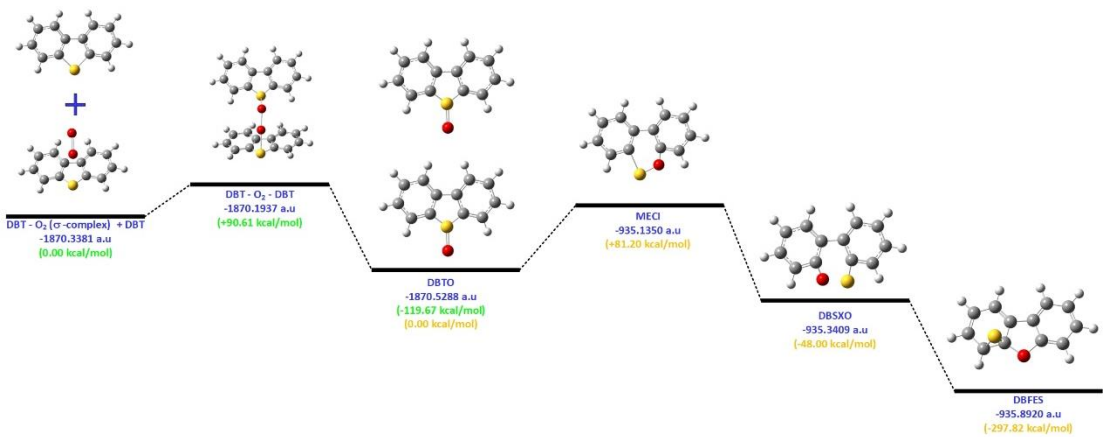

Figure 16: Reaction pathway from $DBTO_2$ (σ -complex) to DBFES and Sn along with its energy profile: Energy values synthesized from $DBTO_2$ (σ -complex) (Green) and DBTO (Orange).

This state is a consequence of DBT absorbing photon energy in red light, thus attracting electrons to regions with higher energy levels. This makes DBT a more reactive compound, facilitating its reaction with oxygen to form $DBTO_2$. $DBTO_2$ was initially generated as an intermediate compound, $DBTO_2$ (π -complex), which is less stable and capable of interacting with other molecules. The result is $DBTO_2$ (σ-complex), which exhibits a more stable sigma bond (Figure 15).

After the formation of $DBTO_2$, sulfur can be separated in the form of sulfur allotrope (Sn). This step is performed when $DBTO_2$ is split into DBTO. The process starts with the reaction of $DBTO_2$ (σ-complex) with another DBT molecule, which forms the DBT-O_2-DBT compound. This compound then decomposes to produce two DBTOs. Allotropic sulfur formation occurs via 1aH-benzo[b]thiireno[2,3-h]benzofuran or dibenzofuran episulfide (DBFES) compounds, which starts with the transformation of DBTO monomers into minimum energy cone intersection (MECI)

compounds. The S-O bond in the MECI structure is broken, resulting in the formation of a new compound structure, namely (Z)-6'-tioxo-[1,1'-bi(cyclohexylidene)]-2',3,4',5 tetraen-2-one (DBSXO). In this structural configuration, the oxygen atom will form a pentacyl group. Instead, the sulfur atom will bind to the benzene group, forming the DBFES compound structure (Figure 16).

In DBFES compounds, the sulfur atom will undergo a release reaction, forming a sulfur allotrope (Sn). This reaction will then produce ono-brominated dibenzofuran (DBF). The activation energy required to release the sulfur allotrope in this reaction is approximately 250,185.6420 kcal/mol. This is the final stage of the sulfur release process from the hydrocarbon-DBT bond in diesel oil (Figure 17).

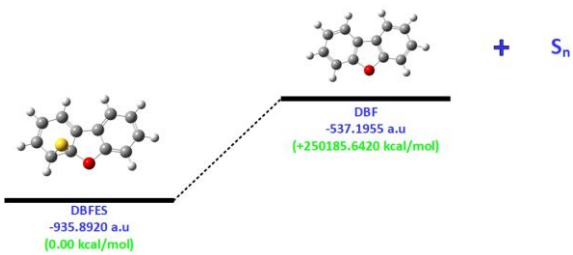

Figure 17: Reaction energy profile of DBF formation and sulfur allotrope from DBFES.

4 Conclusions

The utilization of tin metal in the desulfurization process of diesel oil with red visible light has been shown to play an important role in the reduction of sulfur content, a recent study showed that the use of a catalyst with a height of 6 cm and an irradiation time of 25 hours resulted in the lowest sulfur content of 737 ppm, which shows a significant decrease from the initial value of 1300 ppm. The underlying mechanism of tin metal in this process can be explained through the perspective of photoelectric events. This metal facilitates the enhancement of red visible light energy by increasing the photon energy, frequency, and maximum kinetic energy, while simultaneously reducing its wavelength. FTIR analysis revealed that the cracking of sulfur compounds, especially dibenzothiophene (DBT), occurs through the breaking of C-S bonds, which are the main components in the sulfur structure. In addition, the loss of O-H groups indicates the formation of $DBTO_2$ compounds, which are easier to separate than DBT. Thus, the process is not only effective in reducing sulfur content, but also offers a reaction mechanism that can be optimized for further applications.

Author Contribution

D.D.: investigation, data curation, review, original manuscript writing; I.: investigation, resources; M.D.B: conceptualization, validation; S.H: conceptualization, validation. All author have read and agreed to the published version of the manuscript.

Conflict of Interest

The authors declare no conflict of interest.

Reference

[1] J. L. Holechek, H. M. E. Geli, M. N. Sawalhah, and R. Valdez, "A global assessment: Can renewable energy replace fossil fuels by 2050?," *Sustainability*, vol. 14, no. 8, p. 4792, Apr. 2022, doi: 10.3390/su14084792.

[2] R. Javadli and A. de Klerk, "Desulfurization of heavy oil," *Applied Petrochemical Research*, vol. 1, no. 1–4, pp. 3–19, Mar. 2012, doi: 10.1007/s13203-012-0006-6.

[3] M. Ahmadian and M. Anbia, "Oxidative desulfurization of liquid fuels using polyoxometalate-based catalysts: A review," *Energy & Fuels*, vol. 35, no. 13, pp. 10347–10373, Jul. 2021, doi: 10.1021/acs.energyfuels.1c00862.

[4] T. A. Saleh, *Applying Nanotechnology to the Desulfurization Process in Petroleum Engineering*. Pennsylvania: IGI Global, 2016. doi: 10.4018/978-1-4666-9545-0.

[5] N. Sönnichsen. "Daily Global Crude Oil Demand 2006–2026," Statista.com. https://www.statista.com/statistics/271823/daily-global-crude-oil-demand-since-2006/ (accessed Apr. 15, 2023).

[6] M. Hossain, H. Park, and H. Choi, "A comprehensive review on catalytic oxidative desulfurization of liquid fuel oil," *Catalysts*, vol. 9, no. 3, p. 229, Mar. 2019, doi: 10.3390/catal9030229.

[7] H. Li, Y. Li, L. Sun, S. Xun, W. Jiang, M. Zhang, W. Zhu, and H. Li, "H_2O_2 decomposition mechanism and its oxidative desulfurization activity on hexagonal boron nitride monolayer: A density functional theory study," *Journal of Molecular Graphics and Modelling*, vol. 84, pp. 166–173, Sep. 2018, doi: 10.1016/j.jmgm.2018.

07.002.
[8] I. Shafiq, S. Shafique, P. Akhter, M. Ishaq, W. Yang, and M. Hussain, "Recent breakthroughs in deep aerobic oxidative desulfurization of petroleum refinery products," *Journal of Cleaner Production*, vol. 294, Apr. 2021, Art. no. 125731, doi: 10.1016/j.jclepro.2020.125731.
[9] Y. N. Prajapati and N. Verma, "Hydrodesulfurization of thiophene on activated carbon fiber supported NiMo catalysts," *Energy & Fuels*, vol. 32, no. 2, pp. 2183–2196, Feb. 2018, doi: 10.1021/acs.energyfuels.7b03407.
[10] B. Saha, S. Vedachalam, and A. K. Dalai, "Review on recent advances in adsorptive desulfurization," *Fuel Processing Technology*, vol. 214, Apr. 2021, Art. no. 106685, doi: 10.1016/j.fuproc.2020.106685.
[11] K. X. Lee and J. A. Valla, "Adsorptive desulfurization of liquid hydrocarbons using zeolite-based sorbents: A comprehensive review," *Reaction Chemistry & Engineering*, vol. 4, no. 8, pp. 1357–1386, 2019, doi: 10.1039/C9RE00036D.
[12] P. S. Kulkarni and C. A. M. Afonso, "Deep desulfurization of diesel fuel using ionic liquids: Current status and future challenges," *Green Chemistry*, vol. 12, no. 7, p. 1139, 2010, doi: 10.1039/c002113j.
[13] X. Zhou, T. Wang, H. Liu, X. Gao, C. Wang, and G. Wang, "Desulfurization through photocatalytic oxidation: A critical review," *ChemSusChem*, vol. 14, no. 2, pp. 492–511, Jan. 2021, doi: 10.1002/cssc.202002144.
[14] M. F. Majid, H. F. Mohd Zaid, C. F. Kait, K. Jumbri, L. C. Yuan, and S. Rajasuriyan, "Futuristic advance and perspective of deep eutectic solvent for extractive desulfurization of fuel oil: A review," *Journal of Molecular Liquids*, vol. 306, pp. 1–29. May 2020, Art. no. 112870, doi: 10.1016/j.molliq.2020.112870.
[15] M. H. Ibrahim, M. Hayyan, M. A. Hashim, and A. Hayyan, "The role of ionic liquids in desulfurization of fuels: A review," *Renewable and Sustainable Energy Reviews*, vol. 76, pp. 1534–1549, Sep. 2017, doi: 10.1016/j.rser.2016.11.194.
[16] J. Ye, P. Zhang, G. Zhang, S. Wang, M. Nabi, Q. Zhang, and H. Zhang, "Biodesulfurization of high sulfur fat coal with indigenous and exotic microorganisms," *Journal of Cleaner Production*, vol. 197, pp. 562–570, Oct. 2018, doi: 10.1016/j.jclepro.2018.06.223.
[17] C. N. C. Hitam, A. A. Jalil, and A. A. Abdulrasheed, "A review on recent progression of photocatalytic desulphurization study over decorated photocatalysts," *Journal of Industrial and Engineering Chemistry*, vol. 74, pp. 172–186, Jun. 2019, doi: 10.1016/j.jiec.2019.02.024.
[18] A. A. Aabid, J. I. Humadi, G. S. Ahmed, A. T. Jarullah, M. A. Ahmed, and W. S. Abdullah, "Enhancement of desulfurization process for light gas oil using new zinc oxide loaded over alumina nanocatalyst," *Applied Science and Engineering Progress*, vol. 16, no. 3, Feb. 2023, Art. no. 6756, doi: 10.14416/j.asep.2023.02.007.
[19] O. Morton, "Solar energy: A new day dawning?: Silicon valley sunrise," *Nature*, vol. 443, pp. 19–22, Apr. 2006, doi: 10.1038/443019A.
[20] N. S. Lewis, "Toward cost-effective solar energy use," *Science*, vol. 315, no. 5813, pp. 798–801, Feb. 2007, doi: 10.1126/science.1137014.
[21] D. G. Nocera, "On the future of global energy," *Daedalus*, vol. 135, no. 4, pp. 112–115, Apr. 2006, doi: 10.1162/DAED.2006.135.4.112.
[22] M. A. Gondal, M. N. Siddiqui, and K. Al-Hooshani, "Removal of sulfur compounds from diesel using ArF laser and oxygen," *Journal of Environmental Science and Health - Part A Toxic/Hazardous Substances and Environmental Engineering*, vol. 48, no. 13, pp. 1663–1669, 2013, doi: 10.1080/10934529.2013.815488.
[23] T.-A. Shinozaki, M. Suenaga, Y. Ko, E. Yamamoto, H. Murayama, and M. Tokunaga, "Ultraviolet light-induced decomposition of benzothiophene and dibenzothiophene derivatives for efficient sulfur removal without additives and catalysts," *Journal of Cleaner Production*, vol. 370, Oct. 2022, Art. no. 133402, doi: 10.1016/j.jclepro.2022.133402.
[24] B. D. Ravetz, A. B. Pun, E. M. Churchill, D. N. Congreve, T. Rovis, and L. M. Campos, "Photoredox catalysis using infrared light via triplet fusion upconversion," *Nature*, vol. 565, no. 7739, pp. 343–346, Jan. 2019, doi: 10.1038/s41586-018-0835-2.
[25] N. Sellet, M. Cormier, and J.-P. Goddard, "The dark side of photocatalysis: Near-infrared photoredox catalysis for organic synthesis," *Organic Chemistry Frontiers*, vol. 8, no. 23, pp. 6783–6790, 2021, doi: 10.1039/D1QO01476E.
[26] S. Gisbertz, S. Reischauer, and B. Pieber, "Overcoming limitations in dual photoredox/nickel-catalysed C–N cross-couplings due to catalyst deactivation," *Nature Catalysis*, vol. 3,

no. 8, pp. 611–620, Jul. 2020, doi: 10.1038/s41929-020-0473-6.

[27] I. Pibiri, S. Buscemi, A. P. Piccionello, and A. Pace, "Photochemically produced singlet oxygen: Applications and perspectives," *ChemPhotoChem*, vol. 2, no. 7, pp. 535–547, Jul. 2018, doi: 10.1002/cptc.201800076.

[28] A. A. Ghogare and A. Greer, "Using singlet oxygen to synthesize natural products and drugs," *Chemical Reviews*, vol. 116, no. 17, pp. 9994–10034, Sep. 2016, doi: 10.1021/acs.chemrev.5b00726.

[29] L. Zeng, L. Huang, W. Lin, L.-H. Jiang, and G. Han, "Red light-driven electron sacrificial agents-free photoreduction of inert aryl halides via triplet-triplet annihilation," *Nature Communications*, vol. 14, no. 1, p. 1102, Feb. 2023, doi: 10.1038/s41467-023-36679-7.

[30] K. Rybicka-Jasińska, T. Wdowik, K. Łuczak, A. J. Wierzba, O. Drapała, and D. Gryko, "Porphyrins as promising photocatalysts for red-light-induced functionalizations of biomolecules," *ACS Organic & Inorganic Au*, vol. 2, no. 5, pp. 422–426, Oct. 2022, doi: 10.1021/acsorginorgau.2c00025.

[31] B. F. Buksh, S. D. Knutson, J. V. Oakley, N. B. Bissonnette, D. G. Oblinsky, M. P. Schwoerer, C. P. Seath, J. B. Geri, F. P. Rodriguez-Rivera, D. L. Parker, G. D. Scholes, A. Ploss, and D. W. C. MacMillan, "μmap-red: Proximity labeling by red light photocatalysis," *Journal of the American Chemical Society*, vol. 144, no. 14, pp. 6154–6162, Apr. 2022, doi: 10.1021/jacs.2c01384.

[32] A. Ogura, N. Ichii, K. Shibata, and K. Takao, "Red-light-mediated Barton–Mccombie reaction," *Bulletin of the Chemical Society of Japan*, vol. 93, no. 7, pp. 936–941, Jul. 2020, doi: 10.1246/bcsj.20200087.

[33] P. Seal, J. Xu, S. De Luca, C. Boyer, and S. C. Smith, "Unraveling photocatalytic mechanism and selectivity in PET-RAFT polymerization," *Advanced Theory and Simulations*, vol. 2, no. 6, Jun. 2019, doi: 10.1002/adts.201900038.

[34] W. Qian, "On the physical process and essence of the photoelectric effect," *Journal of Applied Mathematics and Physics*, vol. 11, no. 06, pp. 1580–1597, 2023, doi: 10.4236/jamp.2023.116104.

[35] B. Fan, C. Zhang, J. Chi, Y. Liang, X. Bao, Y. Cong, B. Yu, X. Li, and G. Li, "The molecular mechanism of retina light injury focusing on damage from short wavelength light," *Oxidative Medicine and Cellular Longevity*, vol. 2022, pp. 1–14, Apr. 2022, doi: 10.1155/2022/8482149.

[36] P. R. Bunker, I. M. Mills, and P. Jensen, "The Planck constant and its units," *Journal of Quantitative Spectroscopy and Radiative Transfer*, vol. 237, Nov. 2019, Art. no. 106594, doi: 10.1016/j.jqsrt.2019.106594.

[37] N. Butto, "The origin and nature of the Planck constant," *Journal of High Energy Physics, Gravitation and Cosmology*, vol. 07, no. 01, pp. 324–332, 2021, doi: 10.4236/jhepgc.2021.71016.

[38] Q. Zhu, S. Xiao, Z. Hua, D. Yang, M. Hu, Y. Zhu, and H. Zhong, "Near Infrared (NIR) light therapy of eye diseases: A review," *International Journal of Medical Sciences*, vol. 18, no. 1, pp. 109–119, 2021, doi: 10.7150/ijms.52980.

[39] B. Koo, H. Yoo, H. J. Choi, M. Kim, C. Kim, and K. T. Kim, "Visible light photochemical reactions for nucleic acid-based technologies," *Molecules*, vol. 26, no. 3, p. 556, Jan. 2021, doi: 10.3390/molecules26030556.

[40] M. A. Coronado, G. Montero, C. García, B. Valdez, R. Ayala, and A. Pérez, "Quality assessment of biodiesel blends proposed by the new Mexican policy framework," *Energies*, vol. 10, no. 5, 2017, doi: 10.3390/en10050631.

[41] M. Qasim, T. M. Ansari, and M. Hussain, "Combustion, performance, and emission evaluation of a diesel engine with biodiesel like fuel blends derived from a mixture of Pakistani waste canola and waste transformer oils," *Energies*, vol. 10, no. 7, 2017, doi: 10.3390/en10071023.

[42] H. W. Ryu, Y. S. Kim, J. H. Kim, and I. W. Cheong, "Direct synthetic route for water-dispersible polythiophene nanoparticles via surfactant-free oxidative polymerization," *Polymer*, vol. 55, no. 3, pp. 806–812, 2014, doi: 10.1016/j.polymer.2013.12.056.

[43] X. Li, S. Ai, Y. Huang, C. Huang, W. Yu, and Z. Mao, "Fast and reversible adsorption for dibenzothiophene in fuel oils with metallic nano-copper supported on mesoporous silica," *Environmental Science and Pollution Research*, vol. 28, no. 3, pp. 2741–2752, 2021, doi: 10.1007/s11356-020-10715-1.

[44] F. Dai, Q. Zhuang, G. Huang, H. Deng, and X. Zhang, "Infrared spectrum characteristics and quantification of OH groups in coal," *ACS Omega*, vol. 8, no. 19, pp. 17064–17076, May 2023, doi: 10.1021/acsomega.3c01336.